Title

Kinetic [18F]-Fluoride of the Knee in Normal Volunteers.

Journal

Clinical Nuclear Medicine, 44(5)

ISSN

0363-9762

Authors

Haddock, Bryan
Fan, Audrey P
Jørgensen, Niklas R
et al.

Publication Date

2019-05-01

DOI

10.1097/rlu.0000000000002533

Peer reviewed

HHS Public Access

Author manuscript

Clin Nucl Med. Author manuscript; available in PMC 2020 May 01.

Published in final edited form as:

Clin Nucl Med. 2019 May ; 44(5): 377–385. doi:10.1097/RLU.0000000000002533.

Kinetic [^{18}F]-fluoride of the knee in normal volunteers

Bryan Haddock[1], **Audrey P. Fan**[2], **Niklas R. Jørgensen**[3,4], **Charlotte Suetta**[1,5], **Garry Evan Gold**[2,6,7], and **Feliks Kogan**[2]

[1]Dep. of Clinical Physiology, Nuclear Medicine and PET, Rigshospitalet, Copenhagen University Hospital, Denmark.

[2]Department of Radiology, Stanford University, Stanford, California, USA.

[3]Dep. of Clinical Biochemistry, Rigshospitalet, Copenhagen University Hospital, Denmark

[4]OPEN, Odense Patient data Explorative Network, Odense University Hospital/Institute of Clinical Research, University of Southern Denmark, Odense, Denmark

[5]Geriatric Research Unit, Bispebjerg-Frederiksberg and Herlev-Gentofte, Copenhagen University Hospitals, Denmark

[6]Department of Bioengineering, Stanford University, Stanford, California, USA; Department of Orthopaedic Surgery, Stanford University, Stanford, California, USA.

[7]Department of Orthopaedic Surgery, Stanford University, Stanford, California, USA.

Abstract

Purpose—[^{18}F]-sodium fluoride ([^{18}F]NaF) is a well established bone-seeking agent which has shown promise to assess bone turnover in a variety of disorders, but its distribution in healthy knee joints has not been explored. This study aims to investigate parametric values for [^{18}F]NaF uptake in various bone tissues types of the knee and their spatial distributions.

Methods—Twelve healthy subjects were hand-injected with 92.5 MBq of [^{18}F]NaF and scanned on a 3T PET/MRI system. Listmode PET data for both knees were acquired for 50 min from injection simultaneously with MRI Dixon and angiography data. The image derived input function was determined from the popliteal artery. Using the Hawkins model, Patlak analysis was performed to obtain K_i (K_i^{pat}) values and nonlinear regression analysis to obtain K_i^{NLR}, K_1, $k_3/(k_2+k_3)$, and blood volume. Comparisons for the measured kinetic parameters, SUV and SUVmax were made between tissue types (subchondral, cortical and trabecular bone) and between regional subsections of subchondral bone.

Results—Cortical bone had highest [^{18}F]NaF uptake differing significantly in all measured parameters when compared to trabecular bone and significantly higher SUVmax and K_1 and than subchondral bone. Subchondral bone also had significantly higher SUV, SUVmax and K_i than trabecular bone tissue. Regional differences were observed in K_1 and $k_3/(k_2+k_3)$ values.

Corresponding author: Bryan Haddock, Dep. of Clinical Physiology, Nuclear Medicine & PET, Rigshospitalet Glostrup, Copenhagen University Hospital, Ndr. Ringvej 57, 2600-Glostrup, Denmark.

Conclusion—Quantitative [18F]NaF-PET is sensitive to variations in bone vascularisation and metabolism in the knee joint.

Introduction

[^{18}F]-sodium fluoride ([^{18}F]NaF) is a well-established bone-seeking agent which has shown promise as a marker to study bone turnover in a variety of bone and joint disorders, including the knee [1–4]. Although most often used in oncological examinations, elevated [^{18}F]NaF standardized uptake values (SUV) have been reported to coincide with early disease changes in osteoarthritis [3–5], rheumatoid arthritis [6,7] and to pain [4,5,8,9]. However, SUV only provides a semi-quantitative measure of tracer uptake and is unable to differentiate underlying physiological mechanisms of clinical importance. Fluoride uptake in bone tissue is dependent on a number of factors including perfusion, capillary permeability, and transit times between blood plasma and extracellular fluid. After reaching the bone matrix, fluoride ions either bind by exchanging with hydroxyl groups in the hydroxyapatite-like mineral of bone to form fluoroapatite [10,11] at sites of remodeling and turnover [12–15] or re-enter the bloodstream. Using the Hawkins [16] kinetic model of [^{18}F]NaF uptake (Figure 1), these underlying processes can be quantified by the rate of transit of the $^{18}F^-$ concentration from plasma to the extravascular bone compartment (K_1), the fraction of extravascular $^{18}F^-$ ions binding to the bone matrix ($k_3/(k_2+k_3)$) and the total rate of fluoride clearance from plasma to the bone matrix (K_i). The parameter K_i has been found to have higher sensitivity to treatment response [17–19] than SUV and similar precision in terms of repeatability [19,20]. Further, K_1 has been applied by several groups as a marker for bone vasculature [21–24] while the parameter describing the tracer extraction fraction ($k_3/(k_2+k_3)$), has been used as a marker for bone turnover [23,25].

Although [^{18}F]NaF kinetic modeling has been studied for bone turnover in the upper body, there is little data for parametric values in the healthy knee [1,26,27]. Further, integrated PET/MRI systems have the potential to improve the clinical feasibility of kinetic modelling. Not only is MRI already widely utilized for imaging of joint disorders, but high-resolution MR angiograms can also help obtain the necessary input function of PET tracer delivery without invasive arterial blood sampling [28]. Furthermore, quantitative MRI metrics such as T1rho and T2 relaxation times are able to assess biochemical and structural properties in cartilage, tendons and muscle [29–34]. PET/MRI systems provide a unique opportunity to leverage the extended MRI scanning time for a simultaneous kinetic PET examination and lower radiation dose;combining the advantages of conventional MRI, quantitative MRI, and molecular information from PET. The purpose of this study was to investigate key parametric and semi-parametric values for [^{18}F]NaF uptake in the healthy knee, including K_i, K_1, $k_3/(k_2+k_3)$, SUV and SUVmax, using PET/MRI. The bone tissues investigated included trabecular bone and subchondral bone of the distal end of the femoral bone and tibial head as well as the cortical bone of the femoral and tibial shafts.

Methods

Study Population

12 healthy subjects with no history of musculoskeletal complications (7 females; age: 22–44 years; body mass index 23 ± 3.3 kg/m^2) and having abstained from exercise for 24 hours were hand-injected via an intravenous catheter with 92.5 MBq of [^{18}F]NaF. The study was performed in compliance with the local Institutional Review Board (Stanford University, Administrative Panels for the Protection of Human Subjects) regulations and all subjects provided written consent prior to the study. One subject repeated the trial on three separate days to evaluate reproducibility.

PET/MRI Scanning

Subjects were scanned on a 3T whole-body time-of-flight PET-MR hybrid system (GE Healthcare, Milwaukee, WI). Each subject was positioned feet-first with a 16-channel flexible phased-array receive-only coil (NeoCoil, Pewaukee, WI) around each knee [35]. The coils were used due to their lower attenuation effect on PET photons. Both knees were scanned using one PET bed (field of view = 25 cm) in list mode starting with the injection of NaF for 50 minutes, and all MRI data was acquired simultaneously with PET imaging.

Magnetic resonance angiography data was acquired using a 3D GRE sequence with imaging parameters: TR / TE = 21/2.1 ms, Slices = 18, slice thickness = 1.2 mm, and flip angle = 15°. A 2-point Dixon fat-water T1-weighted spoiled gradient echo MR sequence was acquired for MR-based attenuation correction (MRAC) of PET data [36] with acquisition parameters: TR/TE1/TE2 = 4.1/1.1/2.2 ms; FOV = 50 × 37.5 cm; matrix = 256 × 128; slice thickness/overlap = 5.2/2.6 mm; 120 images/slab; scan time = 18 s.

For calculation of the image derived input function (IDIF), dynamic PET frame times of 40 × 1 s, 13 × 10 s and 23 × 2 min were reconstructed using time of flight (TOF)-ordered subset expectation maximization (OSEM) with 3 iterations and 21 subsets with corrections for decay, attenuation, scatter, random, and dead-time. Time activity curves of bone PET uptake were determined using dynamic PET time frames of 8 × 2 s, 24 × 2 min with the same corrections. A 3 mL venous blood sample was taken 50 min after injection when arterial and venous blood concentrations have equilibrated and measured in a well counter [37].

Image Derived Input function (IDIF) calculation

The IDIF was determined from [^{18}F]NaF activity (kBq/ml) within the popliteal artery of each knee. The artery was segmented automatically from magnetic resonance angiography (MRA) images and a short time-frame PET angiogram during the arterial phase (0–16s after injection) when the tracer is predominantly in the arteries [28]. In order to minimize spill-over artifacts [38], the voxels centered in the middle of the artery were determined for each dynamic PET frame and used for the IDIF. Central voxels were defined by including the voxels in each axial slice within the highest 10% of arterial NaF activity.

Bone segmentations and regions of interest (ROIs)

Using the in-phase, out-of-phase and water images from the Dixon scans, masks covering the femur, patella and tibia were first created by manually drawing regions-of-interest (ROIs) (Figure 2). The bone tissue was then segmented further to create subchondral/cortical bone masks using k-means clustering (4 clustre groups minimised to squared Euclidean distance repeated 4 times with different initial centroids). The long bone of the femur and tibia was identified as the cortical bone 6–8 cm from the centre of the joint space. Trabecular bone ROIs in the tibia and distal end of the femoral bone were drawn for both legs maintaining a minimum of 3 mm distance from the edge of the bone to avoid partial voluming. Thereafter, the subchondral bone of the femur was manually subdivided into 5 regions: trochlea, central and posterior regions of the medial and lateral compartments. Similarly, tibial subchondral bone was further separated into lateral and medial regions. Lastly, cortical bone at the site of a patellar tendon insertion (tibial tuberosity) was identified and excluded from the analysis of cortical bone.

SUV and Kinetic modelling

The time activity curves (TAC) and IDIF data were fitted to the two tissue compartment model using the Patlak method and again using the nonlinear regression (NLR) method. Patlak analysis [27,39] is a graphical technique for estimating K_i, the total rate of plasma clearance of NaF to the bone matrix, that assumes that $^{18}F^-$ is irreversibly bound to bone mineral (k_4=0). Data from 10–50 min were fit to allow for equilibration between tracer in plasma and the bone extracellular fluid. NLR fitting included estimation of 3 rate parameters (K_1, k_2, and k_3) along with a partial volume fraction, a blood fraction and a input dispersion estimate and was computed using COMKAT software [40]. The rate constant k_4 was predefined as 0. For both blood fraction and K_1, a parameter range from 0 to 1 was applied, while a range of 0.015 to 0.8 was used for k_2 and k_3 and 0–2 s for the dispersion constant tau. To avoid local minimums, fits were repeated with three starting conditions and results with the lowest residuals were used. The rate of total plasma clearance using the NLR method (K_i^{NLR}) was calculated from the K_1, k_2 and k_3 values obtained by using the formula:

$$K_i^{NLR} = K_1 * \left(k_3/\left(k_2 + k_3\right)\right) \quad (1)$$

K_i^{NLR}, like K_1, has units of $mL \cdot min^{-1} \cdot mL^{-1}$ whereas $k_2 - k_3$ have units of min^{-1}.

The K_i^{NLR} parameter can be separated into two parameters of physiological interest. One parameter is K_1, the rate of transit of the $^{18}F^-$ plasma concentration into the extravascular compartment and reflects flow delivery of the tracer. Perfusion (F) estimates for each ROI were derived from K_1 values using least squares regression to the Renkin- Crone formula [41]

$$K_1 = F*(1 - \exp(-PS/F)) \quad (2)$$

where the product of permeability and surface area (PS) was assumed to be 0.24, as reported by Piert et al. [21]. The second physiological parameter is the extraction fraction, $k_3 / (k_2+k_3)$, which represents the fraction of $^{18}F^-$ entering the tissue that binds to the bone matrix as opposed to re-entering the bloodstream.

Images for mean SUV and SUVmax were calculated from images obtained by averaging the last 2 frames of the dynamic study (46–50 min).

Statistics

Values across the entire patient cohort are reported as median with interquartile range and p-values are from Student's paired two-tailed t-tests using a threshold for significance of $p<0.05$ after Bonferroni correction for multiple comparisons. Correlations between obtained parameters were analysed using least products linear regression where goodness of fit was evaluated with a Pearson's adjusted R^2 value. Reproducibility between IDIF blood activity and venous blood samples was analysed by calculating the coefficient of variation (CV), reported in percent. Image co-registration, ROI analysis, calculations and statistical analysis were performed with software created in MATLAB 2013b (MathWorks, Natick, MA, U.S.A).

Results

Median parametric values along with interquartile range across all subjects are presented in Table 1. Variations in global [^{18}F]NaF uptake were observed between subjects (Figure 3) with consequently higher or lower SUV values across all three types of bone tissue. Comparisons between the three bone tissue types are shown in Figure 4. Cortical bone had highest [^{18}F]NaF uptake for all measured parameters compared to trabecular bone ($p<0.01$), which had the lowest uptake. SUV and K_i values for subchondral bone were lower than that of cortical bone, but these differences were not significant after correction for multiple comparisons. Subjects had significantly higher SUVmax and K_1 values and a significantly lower extraction fraction in cortical bone compared to subchondral bone. Subchondral bone had significantly higher [^{18}F]NaF uptake (SUV, SUVmax and K_i^{NLR}; $p<0.01$) than trabecular bone tissue.

There was a regional variance in distribution of K_1 and extraction fraction values. The distribution ranged from cortical bone of the shaft which had the highest vascularisation where $K_1 > K_i$ and $k_3/(k_3+k_2) < 1$, to the trochlea and patella region of subchondral bone where $k_3/(k_3+k_2) \simeq 1$ and $K_1 \simeq K_i$ (Figure 5). By visual analysis of K_1 and $k_3/(k_3+k_2)$ maps, a negative gradient of K_1 values can be seen from the femoral and tibial shafts decreasing towards the joint space. A second gradient can be seen as K_1 is higher in subchondral bone and declines towards the centre of the trabecular bone of the femur and tibial head (Figure 6). In the subchondral bone of the femur, K_1 and blood volume values were higher in the posterior section decreasing to the lowest in the trochlea ($p<0.01$). The opposite gradient was observed in the extraction fraction maps, resulting in total metabolism K_i^{NLR} and SUV images that were more spatially uniform.

There were no other significant differences in [^{18}F]NaF uptake parameters between the three bone tissue types or between subregions of subchondral bone. The sites of tendon insertion had elevated SUV values and significantly higher K_i^{NLR} ($p<0.05$) than remaining cortical bone tissue. The vascularisation was lower (K_1 33% less, blood volume 84% lower (both $p>0.01$)) and the extraction fraction higher (($k_3/(k_3+k_2)$) 88% higher $p<0.01$).

K_i^{NLR} values correlated highly with SUV values ($R^2=0.90$). K_i^{pat} values from the Patlak method had a slightly poorer correlation to SUV ($R^2=0.87$) and were 17% lower than those obtained by NLR (Figure 7). The correlation of K_i^{pat} values to K_i^{NLR} values was high ($R^2=0.97$) despite the 17% bias (Figure 7). Using K_1 values from the NLR fit, flow values were obtained and found to be within few percentage points of K_1 values (Table 1). The K_1 values were in the range where $K_1<<PS$ and thereby the condition $F\approx K_1$ applies.

Group average IDIF values at 1, 5, 10, and 50 min were 10.2, 6.0, 4.2 and 2 kBq/ml when normalised to a 100 MBq injection. At 50 min, mean IDIF values were 6% higher than mean venous blood sample values. CV values between venous blood samples and IDIF values measured at 50 min were 8.3%. Repeated injections in one subject had mean CV values of 9% across time points observed between 1 and 50 min. (Figure 8)

Discussion

Semi-quantitative and quantitative values for [^{18}F]NaF uptake in the knee were obtained from healthy subjects using PET/MRI. A large intersubject variation in NaF uptake was observed as there were significant differences in uptake parameters between cortical bone and the subchondral/trabecular bone tissues. Trabecular bone was found to have significantly lower SUV, K_i, K_1 and blood volume values yet a significantly higher extraction fraction than the cortical bone tissue in the shaft of the femur and tibia. Blood volume was the parameter with the largest discrepancy between bone tissues being significantly higher in the shaft compared to subchondral or trabecular bone of the knee. Subjects had higher vascularisation (larger blood volume and higher K_1 values) in the shaft of the femur and tibia declining with a negative gradient towards the joint space reaching the lowest values at the centre of the trabecular bone near the distal end. This K_1 gradient was partially offset by a gradient of increasing extraction efficiency that was significantly lower in the shaft. A similar regional discrepancy was also evident in SUV, SUVmax, and K_i^{NLR}, though to a lesser degree. These parameters, like K_1, were significantly higher in the shaft decreasing in the subchondral bone and trabecular bone of the knee joint in these healthy individuals. Likewise, the sites of tendon insertion of the cortical bone had much lower vascularisation (K_1 and blood volume), yet a net uptake than regular cortical bone due to a high extraction fraction. A similar observation has been made between the spine and humeral bone tissues where low K_1 values in the humeral bone were partially compensated by a higher $k_3 / (k_3+k_2)$ to give a more comparable, yet still significantly lower, K_i value [23,25]. Aside from the K_1 and $k_3 / (k_3+k_2)$ gradients, all other parametric values within the subchondral bone tissue ROIs of subjects were quite homogenous with no significant differences when comparing subchondral sub-regions across the patella, femur and tibia.

K_i^{pat} values from the Patlak method were 17% lower than those obtained by NLR which is a larger bias than previously reported by Siddique et al where K_i^{pat} was 10% lower than K_i^{NLR} in the lumbar vertebrae [17]. Still, K_i^{NLR} values correlated highly with both K_i^{pat} values (R^2=0.97) and SUV (R^2=0.90) with no regional variations in their correlation. Ultimately, this study gives no evidence of meaningful differences in using Patlak or NLR methods to determine K_i as they could be interchanged with a conversion factor. Studies including mean SUV, K_i^{pat} and K_i^{NLR} have found these parameters to have similar reproducibility with coefficients of variation ranging between 9 and 15% [17–20] although K_i^{NLR} had lower reproducibility when k_4 is not limited to 0 when fitting. In this study, SUV, K_i^{pat} and K_i^{NLR} have comparable variance where inter-subject standard deviations are between 43 to 46% of mean values. Despite similar reproducibility, K_i values have been reported to be a more sensitive measure of regional bone metabolism than SUV [17,18,27,42]. In the limbs, where F^- uptake is low, Brenner et al concluded the minimal change of SUV in a patient must be greater than 50% to reliably detect disease or treatment related changes whereas the same diagnosis could be made from a change in K_i of 25% [18,42]. K_i values have also shown to be more sensitive when analysing alterations in subchondral bone of the femur adjacent to cartilage defects [4]. SUVmax values in this study are similar to previously reported mean SUVmax values of 2.44 for the tibia [43] and 2.22 in the femur shaft [44]. SUVmax has been found to correlate well with adjacent cartilage alterations [2,4] and although it had the largest intra-subject variation in this study, it had a relatively lower variance between subjects and greater differentiation between bone tissues (Figure 4). In this study, using non linear regression was advantageous as obtaining K_1 and extraction fraction parameters provided useful information that could not be extracted from K_i alone.

The K_1 values obtained in this study were within a flow dominant regime where it has, theoretically, a linear correlation to blood flow (K_1<<PS). The flow values obtained in this study compare well with measured blood flow in the femoral shaft [45], but lacks a gold standard measure to investigate K_1 as a surrogate flow measure. To date, the most convincing studies to confirm the relationship between blood flow in bone tissue and K_1 for [^{18}F]NaF kinetics have been performed in swine vertebrae [15,21]. Since, authors have reported a poor correlation between K_1 and bone perfusion in studies of the hip of human surgery patients [22] and the forelimbs of healthy rats [46]. Obtaining an estimate of flow would be of great clinical value. Bone perfusion is usually linked to metabolic activity, and varies greatly between different bones and bone regions in the skeleton where the extremities are amongst the lowest [23,25,47]. Perfusion studies using microspheres have shown a reduction of blood flow in bones related to age [47], osteoporosis [48] and reduced endothelium-dependent vasodilation [49].

With regards to this study's aim to report key parametric values for [^{18}F]NaF uptake in the healthy knee, there are several limitations to be considered when interpreting the results. First, the number of subjects is small where results can be skewed by relatively few abnormalities. The range of ages (22–44 yrs) is a period of rather stable bone density in human adults, but factors such as BMI, varus/valgus alignment, disease or activity level could alter the kinetics in bone tissue. Secondly, despite the numerous advantages from combining PET imaging with MRI in knee examinations, there are disadvantages in foregoing the superior information on bone density which CT provides. This information is

valuable in both the attenuation correction of PET data and the segmentation of bone tissue. Dixon based methods, as employed by the scanner in this study, have been shown to underestimate bone [^{18}F]NaF mean SUV by 10% [50] ranging between 0 and 20% depending on location. The subchondral bone would be least affected being close to the bone surface whereas the trabecular bone could have a more pronounced underestimation of SUV due to improper attenuation correction. Likewise, a similar underestimation of K_1 and K_i would be expected although it would be partially offset by a similar underestimation of activity in input function obtained from the popliteal artery. Lastly, the use of an IDIF would best be confirmed by using arterial sampling as a gold standard. In this study, venous samples confirmed the activity of the later phase of the IDIF but not the earlier phase of high activity.

PET/MRI is an optimal dual imaging combination offering the advantages of the high soft tissue contrast and resolution of MRI and the sensitivity of PET. In this study, MRI angiography added the advantage of segmenting the popliteal artery making an automated process to obtain the IDIF possible. The input functions obtained correspond well with literature values for [^{18}F]NaF from arterial sampling [37] and visual inspection of generated ROIs confirmed successful automated segmentation of the popliteal artery. Mean IDIF values 50 min after injection were 6% higher than venous blood samples taken an equilibrium time point, whereas Cook et al found arterial blood samples to be 2% higher than venous blood samples after 24 minutes [25]. With the increased use of NaF in non-oncological studies of the skeleton it has become even more relevant as moderate differences in NaF uptake may be an early indication of bone degradation in diseases such as osteoarthritis (OA) [5]. The combination of PET/MRI reduces the radiation dose significantly in two ways. First by eliminating CT and secondly since the PET data are acquired for the duration of the MRI protocol (which can be up to an hour) the injected dose of ^{18}F-Fluoride can be decreased from a standard clinical dose of 200 MBq to 90 MBq (used in this study) and still retain the same signal-to-noise ratio in PET SUV maps. The effective dose of this study is estimated to be 2.16 mSv [26]. Quantitative MRI techniques have been widely studied to develop robust biomarkers for the early detection and monitoring of OA [5,51] and monitoring of patients having had an ACL injury [32].

Conclusion

In conclusion, this study showed significant variations in regional bone perfusion and metabolism between skeletal tissue types in the knee joint. We have shown the feasibility of using PET/MR to create an accurate image derived input function from the popliteal artery and to conduct a quantitative and semi-quantitative evaluation of bone metabolism in the knee at a low radiation dosage. [^{18}F]NaF PET/MRI is a non-invasive technique that offers an attractive tool to simultaneously estimate bone perfusion and metabolism at clinically relevant sites of the knee.

Acknowledgments

We thank Dr. Mehdi Khalighi and Jorge Guzman for help with development of techniques for hybrid PET/MR imaging. We also thank Dawn Holley and Harsh Gandhi for help running PET/MRI Scans.

CONFLICTS of Interest

This work was funded by GE Healthcare and National Institute of Health (NIH) grants R01EB002524, K24AR062068 and K99EB022634. The funders had no role in study design, data collection, data analysis, data interpretation, writing nor decision to submit the manuscript. Authors FK, AF, and GEG receive research support from GE Healthcare. Authors BH, NRJ and CS have no conflicts of interest to declare.

Bibliography

1. Jadvar H, Desai B, Conti PS. Sodium 18F-fluoride PET/CT of bone, joint, and other disorders. Semin Nucl Med. 2015;45:58–65. [PubMed: 25475379]
2. Kogan F, Fan AP, Monu U, et al. Quantitative imaging of bone-cartilage interactions in ACL-injured patients with PET-MRI. Osteoarthr Cartil. 2018;26:790–796. [PubMed: 29656143]
3. Kogan F, Broski SM, Yoon D, et al. Applications of PET-MRI in musculoskeletal disease. J Magn Reson Imaging. 2018;48:27–47. [PubMed: 29969193]
4. Savic D, Pedoia V, Seo Y, et al. Imaging Bone-Cartilage Interactions in Osteoarthritis Using [(18)F]-NaF PET-MRI. Mol Imaging. 2016;15:1–12. [PubMed: 28654417]
5. Kogan F, Fan AP, McWalter EJ, et al. PET/MRI of metabolic activity in osteoarthritis: A feasibility study. J Magn Reson Imaging. 2017;45:1736–1745. [PubMed: 27796082]
6. Watanabe T, Takase-Minegishi K, Ihata A, et al. (18)F-FDG and (18)F-NaF PET/CT demonstrate coupling of inflammation and accelerated bone turnover in rheumatoid arthritis. Mod Rheumatol. 2016;26:180–187. [PubMed: 26140472]
7. Raynor W, Houshmand S, Gholami S, et al. Evolving Role of Molecular Imaging with (18)F-Sodium Fluoride PET as a Biomarker for Calcium Metabolism. Curr Osteoporos Rep. 2016;14:115–125. [PubMed: 27301549]
8. Kobayashi N, Inaba Y, Tateishi U, et al. Comparison of 18F-fluoride positron emission tomography and magnetic resonance imaging in evaluating early-stage osteoarthritis of the hip. Nucl Med Commun. 2015;36:84–89. [PubMed: 25230054]
9. Draper CE, Quon A, Fredericson M, et al. Comparison of MRI and ^{18}F-NaF PET/CT in patients with patellofemoral pain. J Magn Reson Imaging. 2012;36:928–932. [PubMed: 22549985]
10. Blau M, Ganatra R, Bender MA. 18 F-fluoride for bone imaging. Semin Nucl Med. 1972;2:31–37. [PubMed: 5059349]
11. Narita N, Kato K, Nakagaki H, et al. Distribution of fluoride concentration in the rat's bone. Calcif Tissue Int. 1990;46:200–204. [PubMed: 2106380]
12. Kato K, Nakagaki H, Robinson C, et al. Distribution of fluoride across cementum, dentine and alveolar bone in rats. Caries Res. 1990;24:117–120. [PubMed: 2340541]
13. Ishiguro K, Nakagaki H, Tsuboi S, et al. Distribution of fluoride in cortical bone of human rib. Calcif Tissue Int. 1993;52:278–282. [PubMed: 8467408]
14. Messa C, Goodman WG, Hoh CK, et al. Bone metabolic activity measured with positron emission tomography and [18F]fluoride ion in renal osteodystrophy: correlation with bone histomorphometry. J Clin Endocrinol Metab. 1993;77:949–955. [PubMed: 8408470]
15. Piert M, Zittel TT, Becker GA, et al. Assessment of porcine bone metabolism by dynamic. J Nucl Med. 2001;42:1091–1100. [PubMed: 11438633]
16. Hawkins RA, Choi Y, Huang SC, et al. Evaluation of the skeletal kinetics of fluorine-18-fluoride ion with PET. J Nucl Med. 1992;33:633–642. [PubMed: 1569473]
17. Siddique M, Frost ML, Blake GM, et al. The precision and sensitivity of (18)F-fluoride PET for measuring regional bone metabolism: a comparison of quantification methods. J Nucl Med. 2011;52:1748–1755. [PubMed: 21990579]
18. Brenner W, Vernon C, Muzi M, et al. Comparison of different quantitative approaches to 18F-fluoride PET scans. J Nucl Med. 2004;45:1493–1500. [PubMed: 15347716]
19. Al-Beyatti Y, Siddique M, Frost ML, et al. Precision of ^{18}F-fluoride PET skeletal kinetic studies in the assessment of bone metabolism. Osteoporos Int. 2012;23:2535–2541. [PubMed: 22237817]

20. Frost ML, Blake GM, Park-Holohan S-J, et al. Long-term precision of 18F-fluoride PET skeletal kinetic studies in the assessment of bone metabolism. J Nucl Med. 2008;49:700–707. [PubMed: 18413385]
21. Piert M, Machulla H-J, Jahn M, et al. Coupling of porcine bone blood flow and metabolism in high-turnover bone disease measured by [(15)O]H(2)O and [(18)F]fluoride ion positron emission tomography. Eur J Nucl Med Mol Imaging. 2002;29:907–914. [PubMed: 12111131]
22. Raijmakers P, Temmerman OPP, Saridin CP, et al. Quantification of 18F-Fluoride Kinetics: Evaluation of Simplified Methods. J Nucl Med. 2014;55:1122–1127. [PubMed: 24868107]
23. Frost ML, Blake GM, Cook GJR, et al. Differences in regional bone perfusion and turnover between lumbar spine and distal humerus: (18)F-fluoride PET study of treatment-naïve and treated postmenopausal women. Bone. 2009;45:942–948. [PubMed: 19660584]
24. Nahmias C, Cockshott WP, Belbeck LW, et al. Measurement of absolute bone blood flow by positron emission tomography. Skeletal Radiol. 1986;15:198–200. [PubMed: 3486475]
25. Cook GJ, Lodge MA, Blake GM, et al. Differences in skeletal kinetics between vertebral and humeral bone measured by 18F-fluoride positron emission tomography in postmenopausal women. J Bone Miner Res. 2000;15:763–769. [PubMed: 10780868]
26. Beheshti M, Mottaghy FM, Paycha F, et al. (18)F-NaF PET/CT: EANM procedure guidelines for bone imaging. Eur J Nucl Med Mol Imaging. 2015;42:1767–1777. [PubMed: 26201825]
27. Blake GM, Siddique M, Frost ML, et al. Imaging of site specific bone turnover in osteoporosis using positron emission tomography. Curr Osteoporos Rep. 2014;12:475–485. [PubMed: 25168931]
28. Khalighi MM, Deller TW, Fan AP, et al. Image-derived input function estimation on a TOF-enabled PET/MR for cerebral blood flow mapping. J Cereb Blood Flow Metab. 2018;38:126–135. [PubMed: 28155582]
29. Akella SV, Regatte RR, Gougoutas AJ, et al. Proteoglycan-induced changes in T1rho-relaxation of articular cartilage at 4T. Magn Reson Med. 2001;46:419–423. [PubMed: 11550230]
30. Wheaton AJ, Casey FL, Gougoutas AJ, et al. Correlation of T1rho with fixed charge density in cartilage. J Magn Reson Imaging. 2004;20:519–525. [PubMed: 15332262]
31. Mosher TJ, Zhang Z, Reddy R, et al. Knee articular cartilage damage in osteoarthritis: analysis of MR image biomarker reproducibility in ACRIN-PA 4001 multicenter trial. Radiology. 2011;258:832–842. [PubMed: 21212364]
32. Monu UD, Jordan CD, Samuelson BL, et al. Cluster analysis of quantitative MRI T2 and T1ρ relaxation times of cartilage identifies differences between healthy and ACL-injured individuals at 3T. Osteoarthr Cartil. 2016;25:513–520. [PubMed: 27720806]
33. David-Vaudey E, Ghosh S, Ries M, et al. T2 relaxation time measurements in osteoarthritis. Magn Reson Imaging. 2004;22:673–682. [PubMed: 15172061]
34. Haddock B, Holm S, Poulsen JM, et al. Assessment of muscle function using hybrid PET/MRI: comparison of 18F-FDG PET and T2-weighted MRI for quantifying muscle activation in human subjects. Eur J Nucl Med Mol Imaging. 2017;44:704–711. [PubMed: 27604791]
35. Kogan F, Levine E, Chaudhari AS, et al. Simultaneous bilateral-knee MR imaging. Magn Reson Med. 2018;80:529–537. [PubMed: 29250856]
36. Wagenknecht G, Kaiser H-J, Mottaghy FM, et al. MRI for attenuation correction in PET: methods and challenges. MAGMA. 2013;26:99–113. [PubMed: 23179594]
37. Blake GM, Siddique M, Puri T, et al. A semipopulation input function for quantifying static and dynamic 18F-fluoride PET scans. Nucl Med Commun. 2012;33:881–888. [PubMed: 22617486]
38. Lüdemann L, Sreenivasa G, Michel R, et al. Corrections of arterial input function for dynamic H215O PET to assess perfusion of pelvic tumours: arterial blood sampling versus image extraction. Phys Med Biol. 2006;51:2883–2900. [PubMed: 16723773]
39. Patlak CS, Blasberg RG, Fenstermacher JD. Graphical evaluation of blood-to-brain transfer constants from multiple-time uptake data. J Cereb Blood Flow Metab. 1983;3:1–7. [PubMed: 6822610]
40. Muzic RF, Cornelius S. COMKAT: compartment model kinetic analysis tool. J Nucl Med. 2001;42:636–645. [PubMed: 11337554]

41. Renkin EM. Transport of potassium-42 from blood to tissue in isolated mammalian skeletal muscles. Am J Physiol. 1959;197:1205–1210. [PubMed: 14437359]
42. Apostolova I, Brenner W. Measuring Bone Metabolism with Fluoride PET: Methodological Considerations. PET Clin. 2010;5:247–257. [PubMed: 27157831]
43. Sabbah N, Jackson T, Mosci C, et al. 18F-sodium fluoride PET/CT in oncology: an atlas of SUVs. Clin Nucl Med. 2015;40:e228–31. [PubMed: 25546225]
44. Win AZ, Aparici CM. Normal SUV values measured from NaF18- PET/CT bone scan studies. PLoS ONE. 2014;9:e108429. [PubMed: 25254490]
45. Temmerman OPP, Raijmakers PGHM, Kloet R, et al. In vivo measurements of blood flow and bone metabolism in osteoarthritis. Rheumatol Int. 2013;33:959–963. [PubMed: 22833241]
46. Tomlinson RE, Silva MJ, Shoghi KI. Quantification of skeletal blood flow and fluoride metabolism in rats using PET in a pre-clinical stress fracture model. Mol Imaging Biol. 2012;14:348–354. [PubMed: 21785919]
47. Bloomfield SA, Hogan HA, Delp MD. Decreases in bone blood flow and bone material properties in aging Fischer-344 rats. Clin Orthop Relat Res. 2002;248–257.
48. Griffith JF, Yeung DKW, Tsang PH, et al. Compromised bone marrow perfusion in osteoporosis. J Bone Miner Res. 2008;23:1068–1075. [PubMed: 18302498]
49. Prisby RD, Ramsey MW, Behnke BJ, et al. Aging reduces skeletal blood flow, endothelium-dependent vasodilation, and NO bioavailability in rats. J Bone Miner Res. 2007;22:1280–1288. [PubMed: 17451371]
50. Aznar MC, Sersar R, Saabye J, et al. Whole-body PET/MRI: the effect of bone attenuation during MR-based attenuation correction in oncology imaging. Eur J Radiol. 2014;83:1177–1183. [PubMed: 24780817]
51. Kogan F, Fan AP, Gold GE. Potential of PET-MRI for imaging of non-oncologic musculoskeletal disease. Quant Imaging Med Surg. 2016;6:756–771. [PubMed: 28090451]

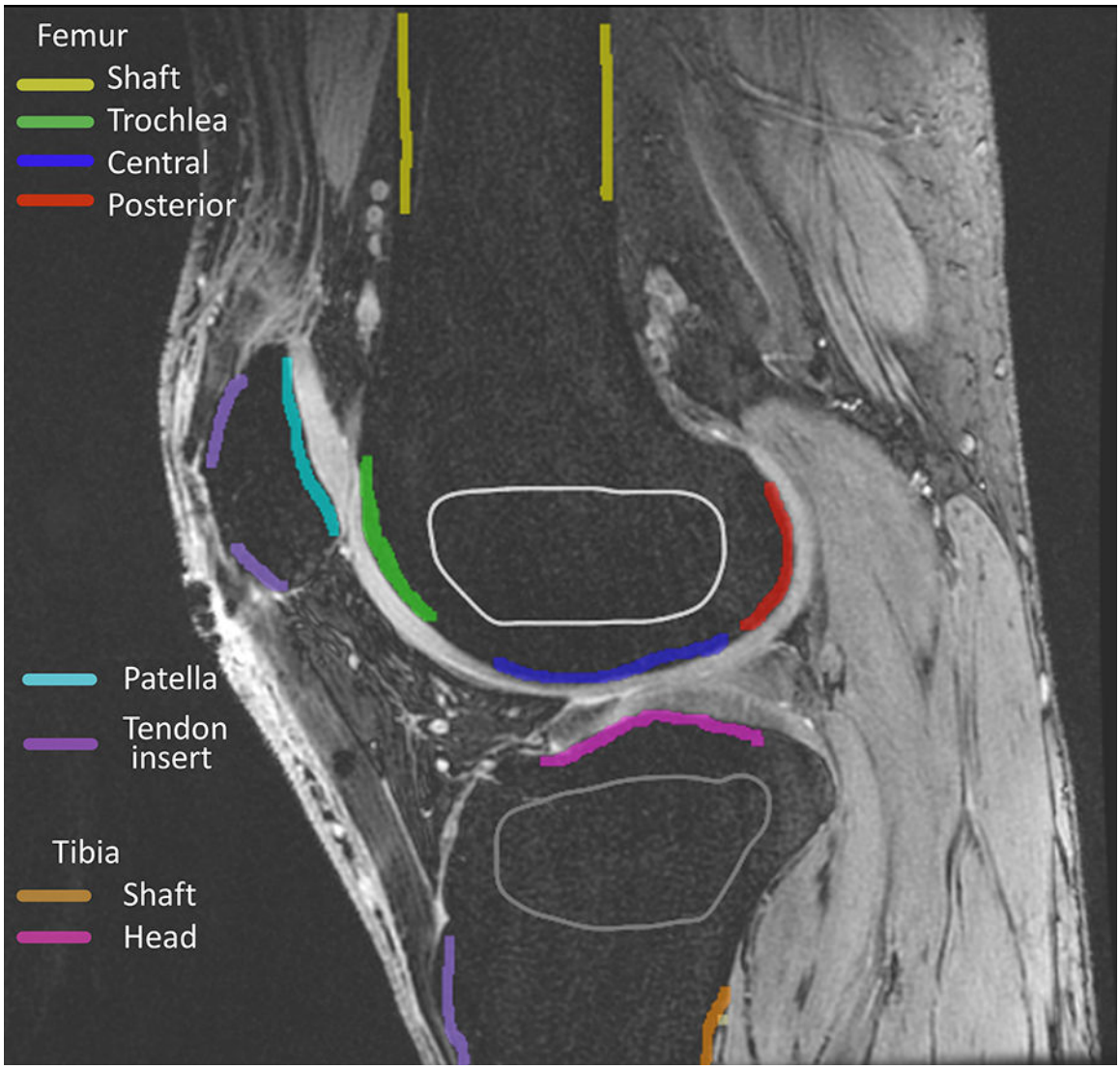

Figure 1. Hawkins two tissue compartment model of [^{18}F]NaF uptake.

The parameter K_1 represents the rate of transit of the $^{18}F^-$ plasma concentration to the extravascular compartment. The accumulating fluoride concentration in bone tissue proceeds from the extravascular compartment by binding to the bone matrix at a rate of k_3 and diffuses back to the blood compartment at a rate defined by k_2. The eventual rate of dissociation of the fluoride from the bone matrix is described by k_4.

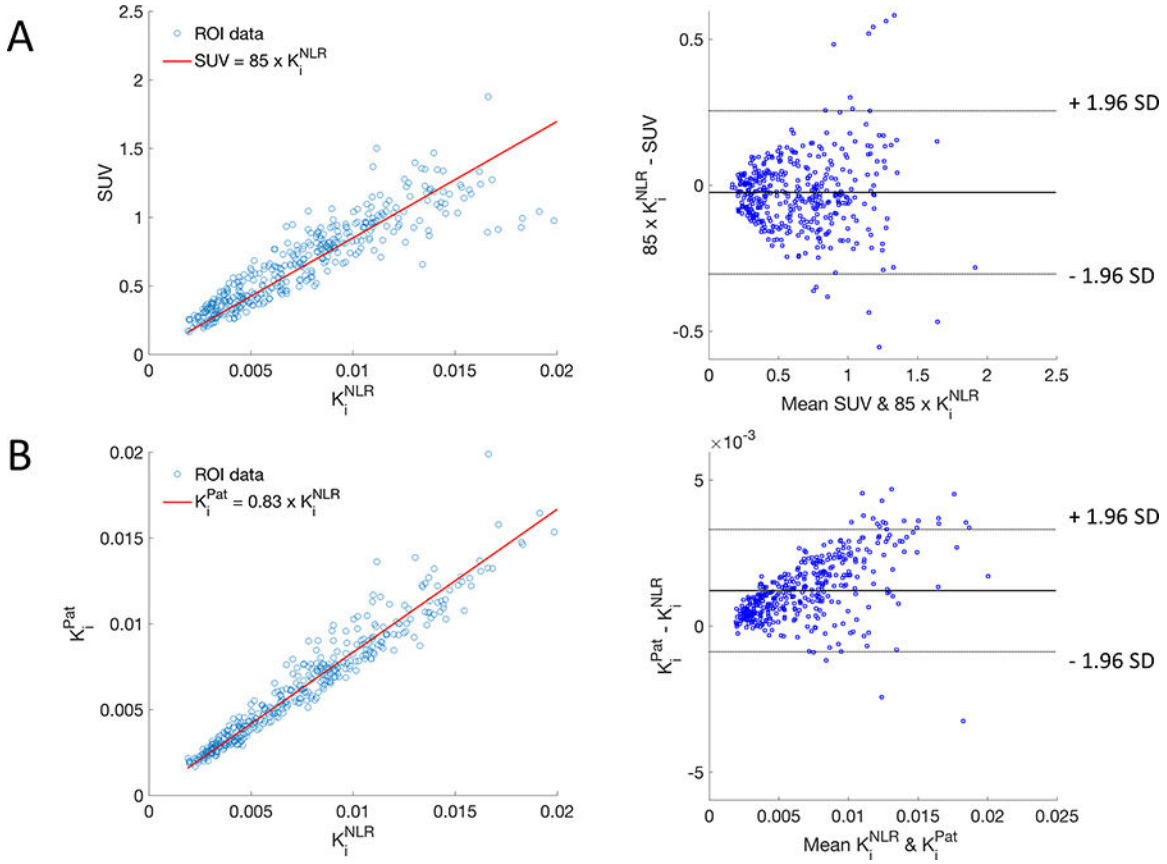

Figure 2. Example of ROIs created in the lateral knee of one subject.

Bone ROIs were generated by segmenting the compact (subchondral and cortical) from trabecular bone tissue using k-means clustering. ROIs were then drawn for the subchondral bone of the patella (teal), tibia (magenta) and the femoral distal end which was subdivided into trochlear (green), central (blue) and posterior (red) sections. Trabecular bone was segmented in the femur and tibia by manually drawing ROIs keeping a minimum distance of 3mm from subchondral bone (shown as light grey in the femur and dark grey in the tibia). ROIs were created for cortical bone in the femoral (yellow) and tibial shaft (orange). Lastly, a separate set of cortical ROIs were drawn for the cortical bone at the sites of tendon insertion (purple) on the patella and tibia.

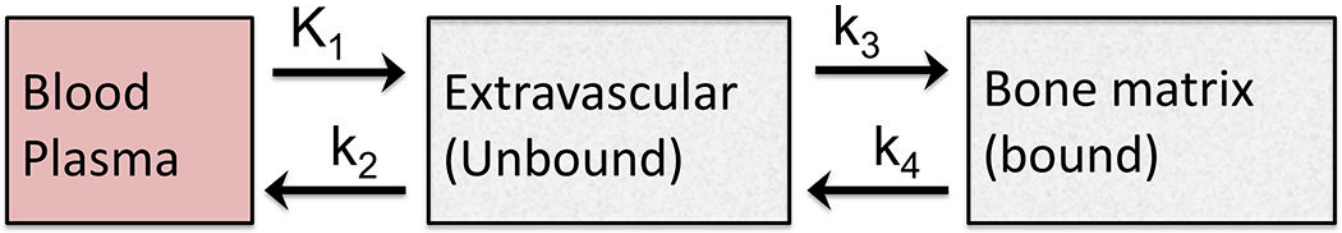

Figure 3. Standardized uptake value (SUV) of representative slice from 2 subjects.

There was a wide intersubject range of [^{18}F]NaF uptake across the joint. The left image is a subject with low uptake in knee while the right image is a subject with high uptake in all bone tissues. In addition to global variations in tracer uptake between subjects, some individual variations in the relative distribution of [^{18}F]NaF uptake across bone tissues regions were observed. In this example, the subject on the right has relatively low uptake in the subchondral bone of the femur compared to the subchondral bone of the patella and tibial head whereas the subject on the left has equally low uptake in all subchondral regions.

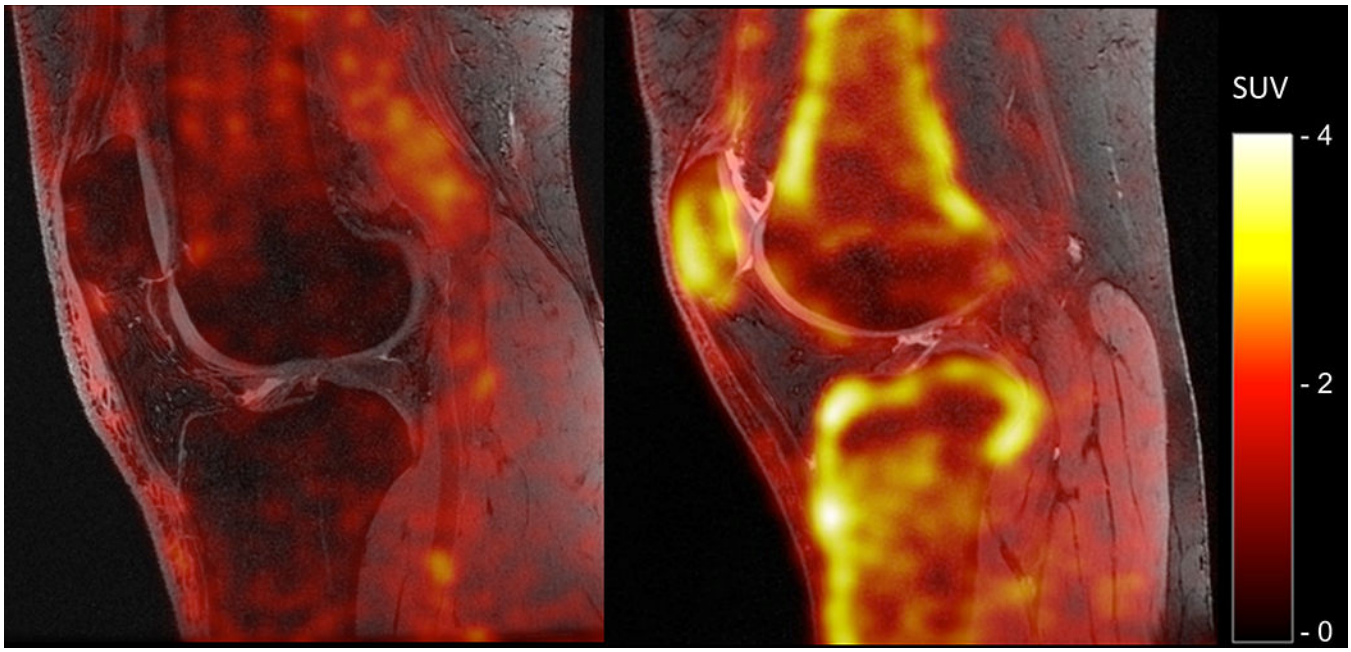

Figure 4. Parametric values of [^{18}F]NaF uptake for different bone tissue types of the knee.

Cortical bone had the highest [^{18}F]NaF uptake in all measured parameters when compared to trabecular bone, which had the lowest uptake. Subchondral bone also had higher uptake than trabecular bone with significantly higher SUVmean, SUVmax and K_i^{NLR} values, yet only slightly elevated K_1 and $k_3/(k_3+k_2)$ values. The relative distribution of K_i^{NLR} values between bone tissues was almost identical to that of SUV. Note that despite having the highest uptake as expressed by SUV and K_i^{NLR}, cortical bone has the lowest extraction fraction. P values were corrected for 18 comparisons using a Bonferroni correction. († $p<0.01$ difference compared to cortical bone, ‡ $p<0.01$ difference between trabecular bone and subchondral bone)

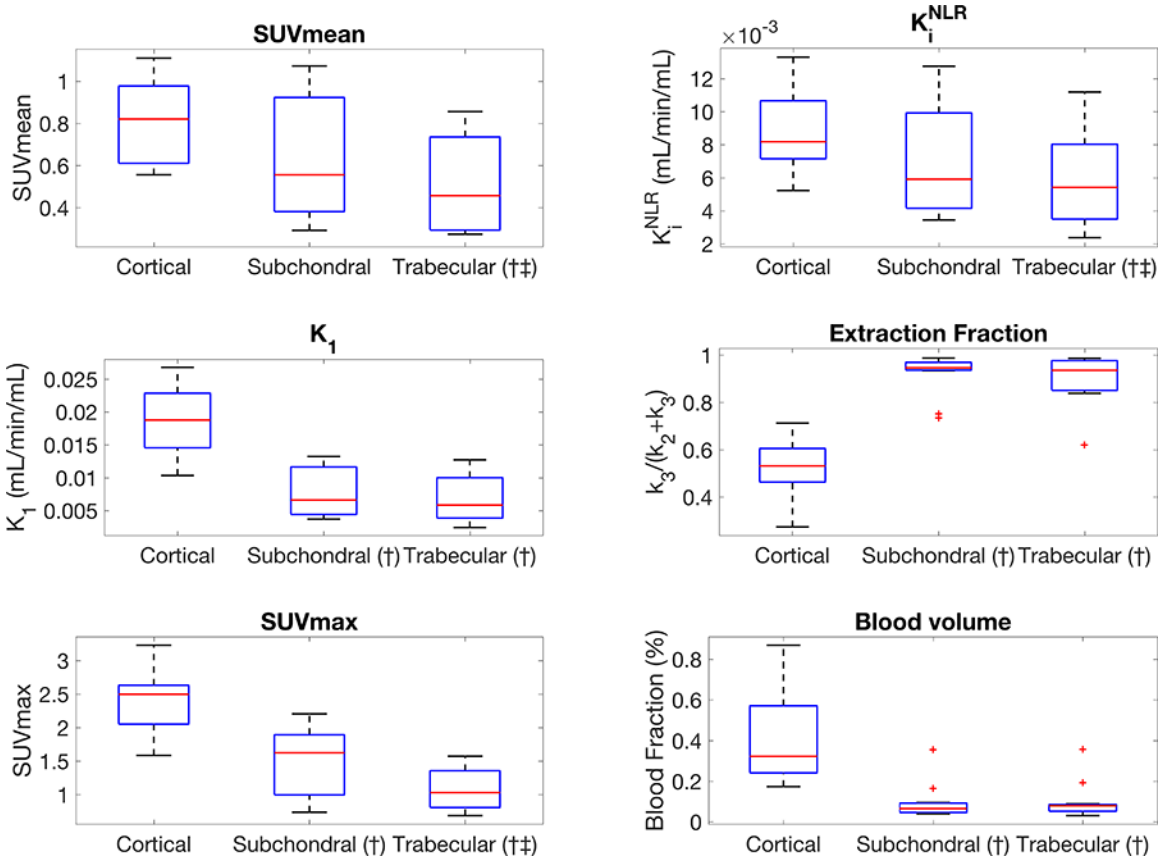

Figure 5. Components of K_i for different bone tissue type.

The SUV / K_i^{NLR} relationship did not vary significantly between tissue types nor between subjects. Linear regression analysis of SUV and K_i^{NLR}gave SUV= 89 × K_i^{NLR}. The first column compares different ROI values from all subjects to this regression. Given that K_i=K_1 × $k_3/(k_3+k_2)$, K_i can be broken into a flow-related K_1 component, which is the rate of tracer entering the tissue, and an extraction fraction component, $k_3/(k_3+k_2)$, which is the fraction of the tracer having entered the tissue that binds to the bone matrix. SUV of the cortical bone (shaft) is correlated to both K_1 and $k_3/(k_3+k_2)$ values, whereas in trabecular bone and the patella, SUV is primarily determined by K_1 where $K_i \simeq K_1$ and $k_3/(k_3+k_2) \simeq 1$ in all subjects.

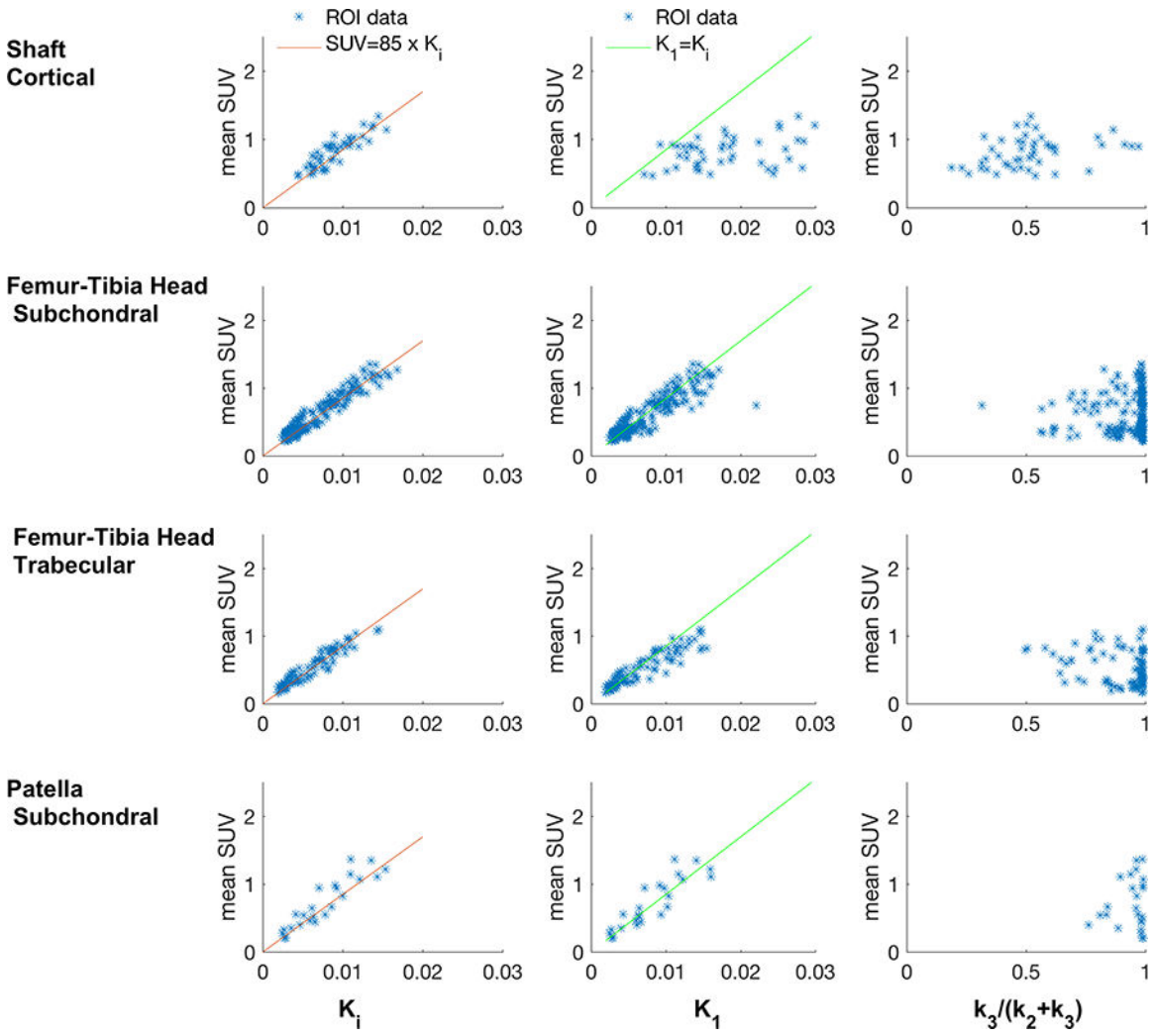

Figure 6. Example of the distribution of K_1, K_i^{NLR} and SUV from one subject

Subjects had a negative gradient of K_1 values from the shaft towards the joint space and from the subchondral bone towards the centre of the distal end of the femoral bone and tibial head. In the sagittal plane K1 values were highest in the posterior section of subchondral bone and decreased in the anterior direction towards the trochlea and patella. However, the opposite gradient was observed in extraction fraction $k_3 / (k_2+k_3)$ maps, resulting in K_i^{NLR} and SUV images with more localised heterogeneity.

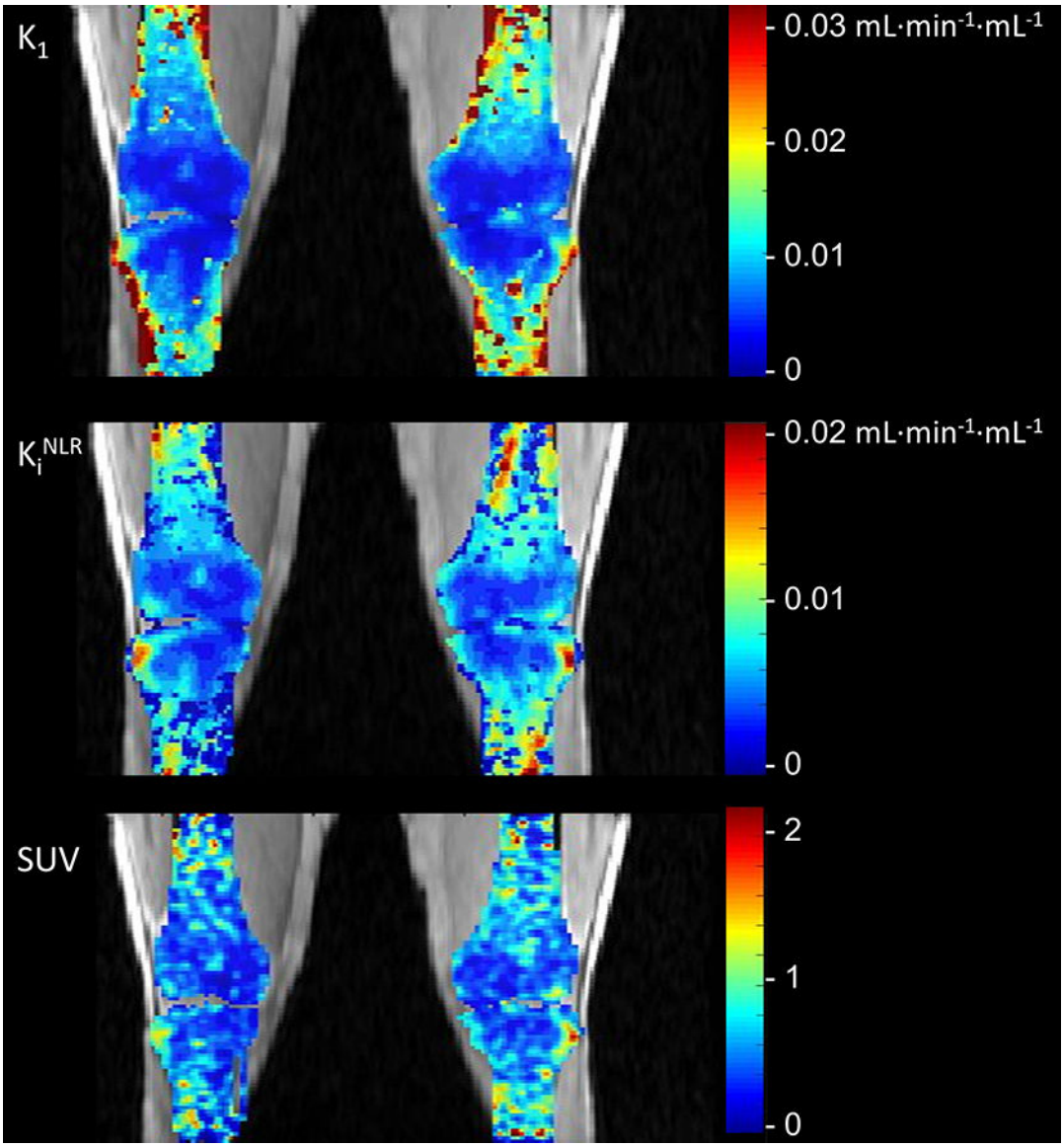

Figure 7. Comparison of K_i^{NLR} with SUV values and Kipat Patlak

A: Scatter plot of K_i^{NLR} results from all ROIs of all subjects plotted against ROI mean SUV (R^2=0.90). The Bland-Altman plot compares SUV values and K_i^{NLR} values multiplied by the slope determined from the regression (slope=90). B: A scatter plot with regression fit and Bland-Altman plot of the same ROIs comparing K_i^{NLR} vs K_i^{pat} values (R^2=0.97). The Patlak method produced K_i values that were 17% lower than those obtained by NLR and had a slightly poorer correlation to SUV (R^2=0.87).

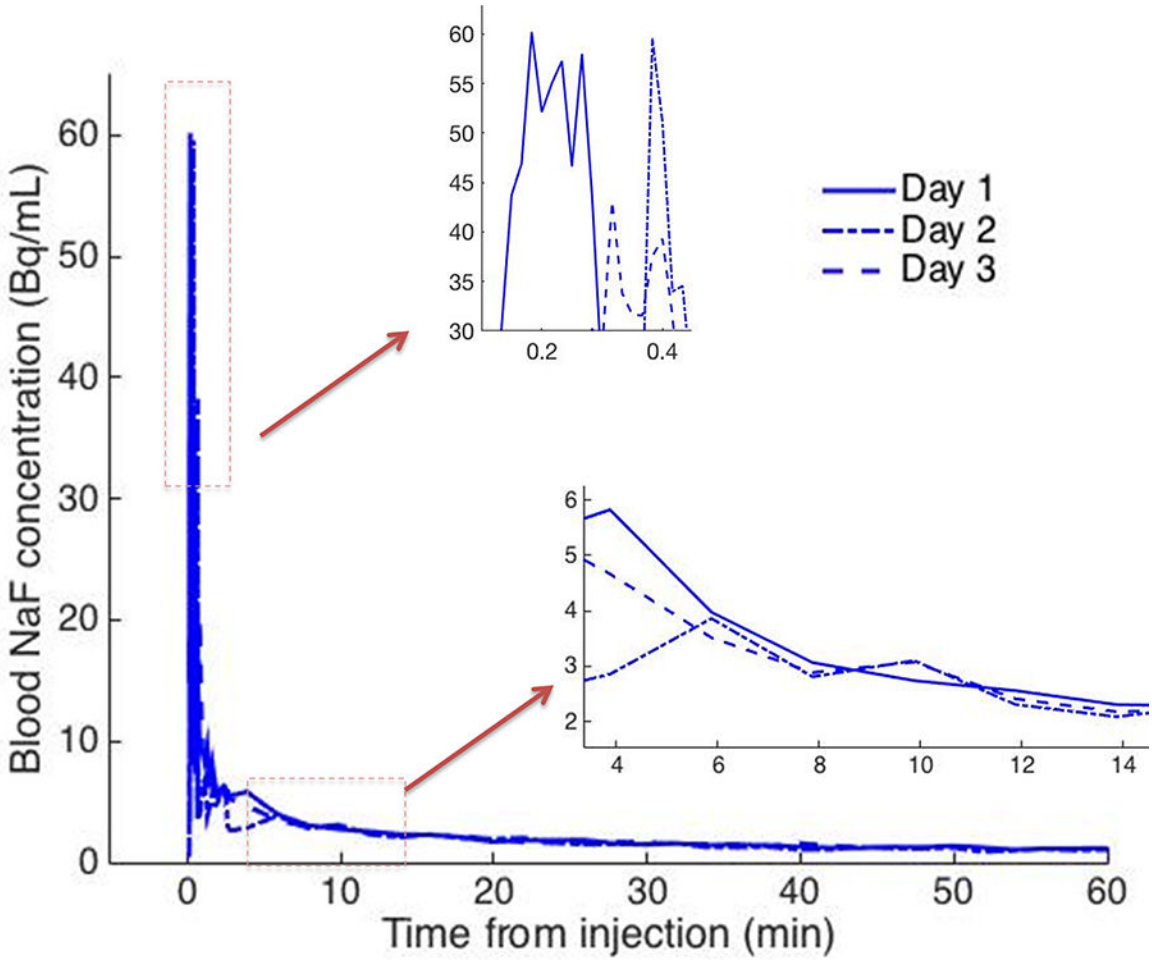

Figure 8. Image derived input function of [^{18}F]NaF repeated in one subject.

One subject underwent injections on three separate days. IDIFs for each scan are plotted from time of injection. Reproducibility across sessions was good with an average coefficient of variation of 9% between 1 and 50 min.

Table 1

Parametric values for bone tissues of the patella, tibia and femur.

Median parametric values from different bone tissue with interquartile range in parenthesis. Measures are further divided into the tibial, femoral and patellar bones. Comparisons between tissue types are shown in figure 4. There were no significant differences for a given tissue type between the three bones.

	Patella -Subchondral	Femur-Subchondral	Tibia-Subchondral	Tendon insert	Femur- Cortical (Shaft)	Tibia-Cortical (Shaft)	Femur-Trabecular	Tibia- Trabecular
SUV	0.7 (0.43 – 1.02)	0.52 (0.38 – 0.94)	0.52 (0.37 – 0.85)	0.89 (0.58 – 1.14)	0.78 (0.55 – 1.03)	0.84 (0.7 – 0.91)	0.4 (0.27 – 0.79)	0.52 (0.35 – 0.71)
SUV_{max}	1.93 (1.18 – 2.59)	2.49 (1.91 – 3.11)	1.98 (1.35 – 2.54)	3.0 (2.09 – 4.6)	3.12 (2.51 – 3.62)	2.24 (1.91 – 2.8)	1.35 (0.85 – 1.73)	1.4 (1.12 – 1.63)
K_i^{NLR} mL/min/mL $\times 10^{-2}$	0.81 (0.44 – 1.09)	0.56 (0.43 – 1.0)	0.6 (0.4 – 0.93)	1.07 (0.72 – 1.4)	0.82 (0.61 – 1.1)	0.87 (0.76 – 0.98)	0.43 (0.27 – 0.82)	0.58 (0.41 – 0.81)
K_1 mL/min/mL $\times 10^{-2}$	0.86 (0.52 – 1.13)	0.66 (0.47 – 1.17)	0.64 (0.41 – 1.04)	1.29 (0.74 – 1.6)	1.67 (1.22 – 2.42)	1.88 (1.34 – 2.19)	0.44 (0.29 – 0.94)	0.67 (0.46 – 1.11)
$\frac{k_3}{k_3 + k_2}$	0.97 (0.91 – 0.99)	0.95 (0.92 – 0.97)	0.98 (0.92 – 0.99)	0.95 (0.9 – 0.96)	0.51 (0.43 – 0.61)	0.48 (0.41 – 0.56)	0.98 (0.94 – 0.99)	0.89 (0.78 – 0.98)
K_i^{pat} mL/min/mL $\times 10^{-2}$	0.69 (0.38 – 0.99)	0.51 (0.33 – 0.9)	0.5 (0.34 – 0.81)	0.94 (0.64 – 1.31)	0.62 (0.48 – 0.95)	0.67 (0.58 – 0.77)	0.38 (0.23 – 0.73)	0.49 (0.33 – 0.63)
Perf mL/min/mL $\times 10^{-2}$	0.86 (0.52 – 1.13)	0.66 (0.47 – 1.17)	0.64 (0.41 – 1.04)	1.29 (0.74 – 1.6)	1.67 (1.22 – 2.42)	1.88 (1.34 – 2.19)	0.44 (0.29 – 0.94)	0.67 (0.46 – 1.11)
Blood (%vol)	0.04 (0.03 – 0.06)	0.07 (0.05 – 0.13)	0.05 (0.03 – 0.07)	0.05 (0.04 – 0.06)	0.38 (0.22 – 0.64)	0.35 (0.27 – 0.48)	0.06 (0.04 – 0.08)	0.09 (0.06 – 0.12)